



# Effect of heat treatment parameters on microstructure evolution, tensile strength, wear resistance, and fracture behavior of Ni–Ti multilayered composites produced by cross-accumulative roll bonding

Qing Ye<sup>1</sup> · Xuejun Li<sup>2</sup> · Moslem Tayyebi<sup>3</sup> · Amir Hossein Assari<sup>4</sup> · Adelajda Polkowska<sup>5</sup> · Sebastian Lech<sup>6</sup> · Wojciech Polkowski<sup>5</sup> · Morteza Tayebi<sup>7</sup>

Received: 23 June 2022 / Revised: 7 October 2022 / Accepted: 22 October 2022 / Published online: 14 November 2022  
© Wrocław University of Science and Technology 2022

## Abstract

The last decades have seen a huge growth in the investigation of intermetallic compounds at the interfaces of laminated composites due to their useful features. In this research, effects of the formation of intermetallic compounds on tensile properties and wear resistance of Ni/Ti composites produced by cross-accumulative roll bonding (CARB) process have been examined at different annealing times and temperatures. Scanning electron microscopy (SEM) images demonstrated that the layers were well bonded together, but Ni layers experienced instabilities in light of plastic deformation. The EBSD results showed lamellar structure and crystallographic texture on Ti and Ni layers during plastic deformation. According to X-ray diffractometer (XRD) and energy-dispersive spectrometer (EDS) analyses, NiTi<sub>2</sub> and NiTi were present in all annealed samples. The thickness of intermetallic compounds grew with an increase in annealing temperature and time. However, this growth led to a decrease in tensile strength while the values of elongation fluctuated. Based on the results of the wear test, the composite became more resistant to wear when the thickness of intermetallic layers increased. The surfaces of these layers with less roughness and lower coefficients of friction facilitated the movement of steel pin on samples during the wear test. Furthermore, wear mechanisms of adhesion, abrasion, and delamination were observed, and they were more noticeable at higher loads and lower annealing temperatures and times.

**Keywords** Intermetallic compounds · Laminated composite · Wear test · Mechanical properties · Annealing treatment · Fracture

## 1 Introduction

The importance of bonding dissimilar metallic materials during the last decade has led to the recent development in the field of manufacturing multilayered composites [1–6]. Many

technologies have been utilized, namely diffusion bonding [7], explosive welding [8], and roll bonding [9]. However, some of these fabrication methods suffer from their expensive tools. Therefore, accumulative roll bonding (ARB) process [10, 11] which is a severe plastic deformation (SPD) method has

✉ Qing Ye  
zq375496861@126.com

✉ Moslem Tayyebi  
moslemtayyebi1990@gmail.com

<sup>1</sup> School of Mechanical Engineering, Xijing University, Xi'an 710123, ShaanXi, China

<sup>2</sup> School of Electronic Information, Xijing University, Xi'an 710123, ShaanXi, China

<sup>3</sup> Department of Materials Science and Engineering, Shiraz University of Technology, Modarres Blvd, Shiraz 71557-13876, Iran

<sup>4</sup> Department of Materials Science and Engineering, Sahand University of Technology, Tabriz, Iran

<sup>5</sup> Łukasiewicz Research Network-Krakow Institute of Technology, Zakopia Nska 73 Street, 30-418 Kraków, Poland

<sup>6</sup> AGH University of Science and Technology, International Centre of Electron Microscopy for Materials Science and Faculty of Metals Engineering and Industrial Computer Science, Mickiewicza 30 Avd, 30-059 Krakow, Poland

<sup>7</sup> Young Researchers and Elites Club, Science and Research Branch, Islamic Azad University, Tehran, Iran

recently emerged in this research area. Several multilayered composites have been produced through the ARB process, such as Cu/Al/Ni [9], Al/Cu [11], and Ni/Ti. The Ni/Ti composite which is composed of magnetic (Ni) and non-magnetic (Ti) constituents is widely used in many areas such as soft X-rays and neutron optics. In addition to their shape memory effects which have been commonly discussed, the Ni/Ti multilayered composites represent better physical and mechanical properties compared with their constituents [12]. Further, the formation of intermetallic compounds at the interface of Ni/Ti has attracted much attention. Indeed, these compounds possess interesting properties and their formation often takes place on account of the interdiffusion of Ni and Ti. For instance, Ding [13] reported the formation of the NiTi phase as a result of a solid-state interdiffusion reaction at a long annealing time in a cold-rolled Ni/Ti composite. On the other hand, it may seem that applying severe plastic deformation on layers before any further heat treatment has an effect on the formation of phases. For example, Zhang [14] studied the effect of low annealing temperatures on the interfacial evolution phases at the interface of Ti/Ni multilayered composites synthesized by the ARB process and found out two phases including NiTi and NiTi<sub>2</sub>. However, unlike Ni–Ti alloys, these composites represent good wear resistance. This feature can be even enhanced after annealing treatment, so that these multilayered composites can be used in severe environments. This is due to the fact that the formation of intermetallic compounds at the interfaces can significantly improve the wear resistance of composites [15, 16]. Although there are a lot of reports on the evolution of microstructure and interfacial phases at different annealing temperatures and times, there is still limited research on the dependence of heat treatment on mechanical properties.

Recently, cross-accumulative roll bonding (CARB) has been frequently utilized to fabricate multilayered composites, especially when their mechanical properties are important. This is because, in this method, after each rolling pass, the rolling direction is rotated 90° around normal direction, thus hindering the probable crack propagation within the composite [17].

Considering the advantages and the significant uses of Ni/Ti composites in industry, for the first time, in this research, the multilayered composites were produced by the CARB process. Next, their kinetics of phase formation and mechanical properties at different annealing temperatures and times were discussed in detail.

## 2 Experimental procedures

### 2.1 Materials and fabrication process

The Nickel (0.5 mm thickness) and Titanium (1 mm thickness) sheets with the purity levels of 99.8% and the same

dimensions of 15 cm × 6 cm were used to fabricate Ni/Ti multilayered composites. They were supplied by Sahand Company Inc. The sheets were first cleaned and steel-brushed, and then, they were stacked alternatively to make Ni/Ti/Ni/Ti/Ni/Ti sandwiches.

To fabricate composites using the cross-accumulative roll bonding (CARB) process, GCr15 roll mills with the load capacity, diameter, and rotation speed of 30 ton, 50 cm, and 10 r/min, respectively, were used. First, the sandwiches were subjected to 66% thickness reduction by roll bonding. Second, after cutting the specimen in two halves, followed by surface preparation, the halves were stacked together and were then subjected to 50% thickness reduction with 90° rotation around the normal direction (ND). Third, the previous stage was repeated one more time. Finally, after three passes, the Ni (50.3wt)/Ti (49.7wt) multilayered composites were achieved, as illustrated in Fig. 1.

To perform annealing treatment, after encapsulating the samples in quartz tubes, they were isothermally annealed at 650, 750, and 850 °C, for 6, 8, and 10 h in an electric furnace (Azar Furnace) with argon atmosphere, followed by air cooling (about 50 °C/min cooling rate).

### 2.2 Microstructural investigation

#### 2.2.1 SEM, EDS, and XRD analyses

The samples were mount, grinded, and polished, respectively. After that, their cross-sections on the ND-RD plane were examined by scanning electron microscope (SEM) equipped with an energy-dispersive spectrometer (EDS) and X-ray diffractometer (XRD—Cu Target, 40 kV and 40 mA) to study the microstructure and the evolution of intermetallic layers.

#### 2.3 EBSD analysis

Microstructural and microtextural features of Ti–Ni samples in the cold deformed conditions were evaluated using FEI Scios™ field emission gun scanning electron microscope (FEG SEM) coupled with TSL automatic electron backscatter diffraction system (EBSD). The analyses were performed on hot-mounted longitudinal sections of samples. The metallographic preparation was carried out by means of mechanical grinding with SiC papers followed by mechanical polishing with 3–0.25 μm diamond suspensions; and then final polishing with silica slurries. Furthermore, to remove surface oxides from Ti, chemical etching with (10% vol. HF + 45% vol. HNO<sub>3</sub> + 45% vol. H<sub>2</sub>O<sub>2</sub>) reagent was applied. Several EBSD scans were performed on mid-thickness areas using a step size of 0.05–0.16 μm to obtain at least 30,000 measurement points in each run. By taking into account a strain-induced

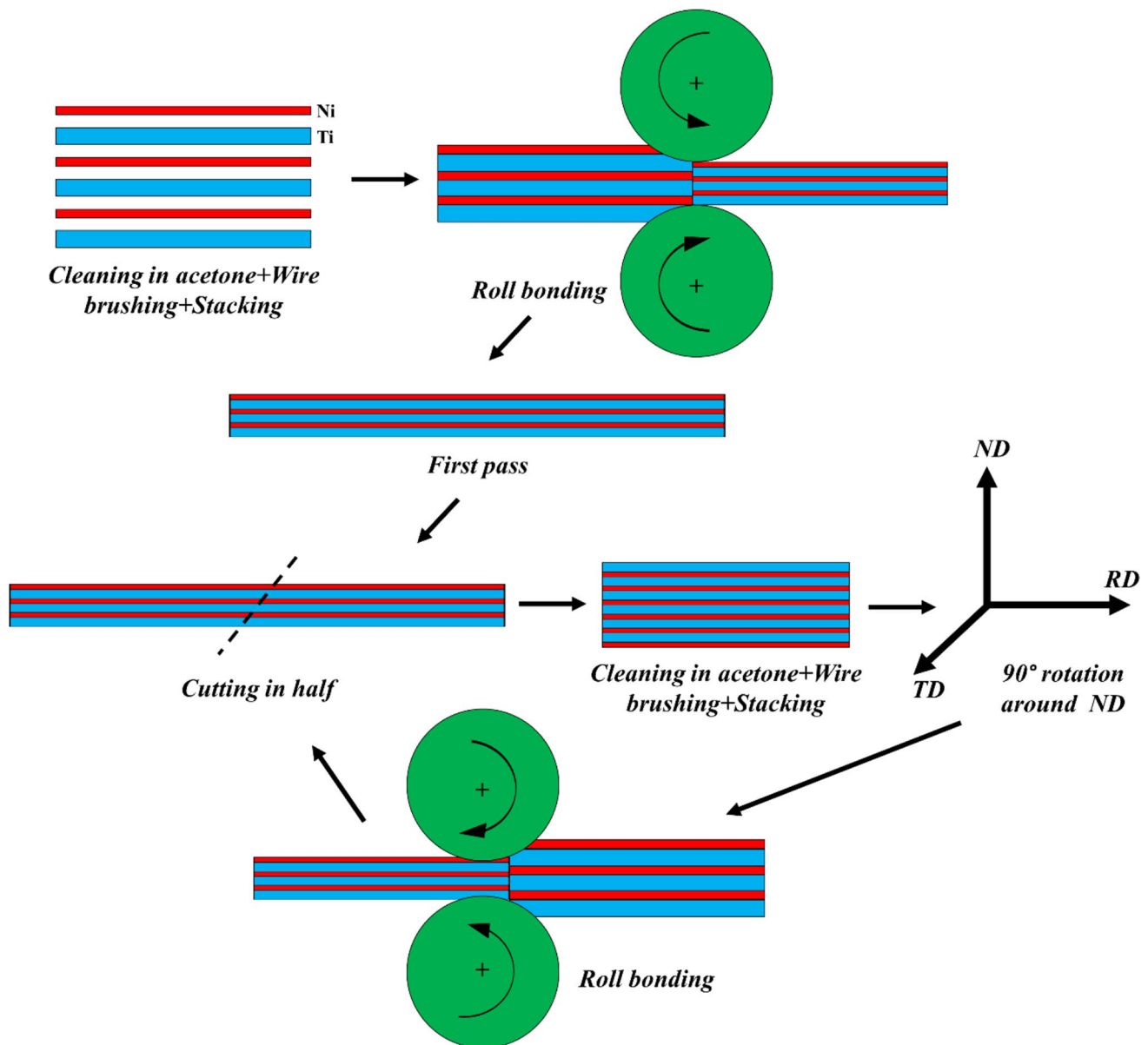


**Fig. 1** Schematic of Ni/Ti sandwich and CARB process

distortion of crystal lattices of involved phases, raw diffraction data were subjected to a post-processing “cleaning” to remove the “noise” effect from the as-received scans. In this regard, points with the neighbor to neighbor confidence index (CI) lower than 0.2 were excluded from the analysis [18]. The crystallographic texture was calculated from acquired EBSD data by computing orientation distribution functions (ODFs). During calculations, Harmonic Series Expansion method and orthonormal sample symmetry have been assumed.

## 2.4 Tensile analysis

According to ASTM E8/E8M-9 standard, the samples were wire-cut. The dimensions of a sample are depicted in Fig. 2. Thereafter, at room temperature and strain rate of  $11 \times 10^{-4} \text{ s}^{-1}$ , uniaxial tensile test was performed on each sample using an Instron tensile test machine equipped with extensometer by which force–displacement curves were measured. Besides, scanning electron microscope (SEM) was employed to characterize the fracture surfaces.

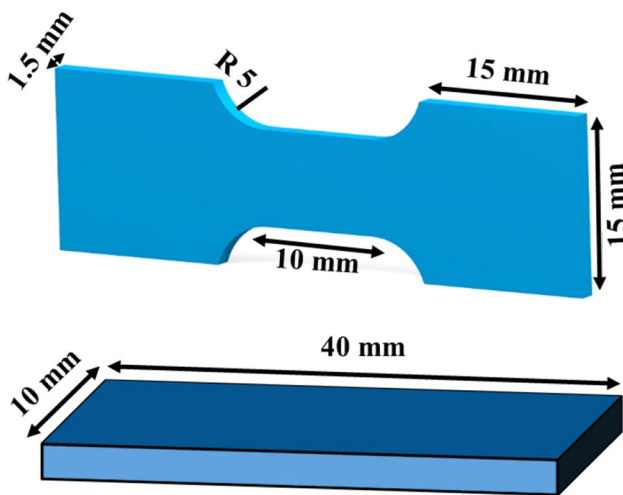


Fig. 2 Schematic of samples used for tensile and wear tests

## 2.5 Wear analysis

To examine the wear mechanisms, the samples were first wire-cut into  $4 \times 1$  cm plates, as illustrated in Fig. 2. Then, their contact surfaces were grinded by SiC papers. After that, based on ASTM G133 standard, reciprocating steel pin-on-plate dry sliding test was performed, at room temperature, on the prepared samples. Wear loads of 10, 100, and 200 N were vertically applied on prepared samples by steel pins with a diameter of 6 mm and the hardness of 60 HRC. Afterward, the weight loss was measured and reported. The roughness of surfaces was also investigated by profilometer on wear tracks. And eventually, the worn surfaces were investigated through a scanning electron microscopy (SEM).

## 3 Results and discussion

### 3.1 Microstructural investigation

Figure 3 shows the microstructure of the as-CARBed sample on ND-RD section. It can be seen that there are two distinct layers across the Ti/Ni laminated composite. The bright grey region represents Ni and the dark grey region shows Ti. The interfaces illustrate good bonding with no apparent cracks or detachment. However, from Fig. 3(b) which displays the sample annealed at 650 °C for 6, 8, and 10 h, consistent interfacial layers at the interfaces of Ti/Ni can be observed which indicates the formation of intermetallic compounds due to the interdiffusion of Ti and Ni atoms. Interestingly, despite the brittleness of these phases, there are no evident cracks or voids adjacent to their interfaces. These observations are in complete agreement with previously published papers [7, 9, 17, 19].

From Fig. 3a and b, necking and shear bonds can be seen. Necking often takes place when the layer is strain hardened in the composites, but shear bands which are at an angle of about 35 degrees with respect to the rolling direction can be seen as a result of the non-uniform strain during roll bonding. It is widely accepted that the formation of these bands is dependent on different parameters, namely the deformation conditions, and the chemical composition of the material [17].

Figure 4 shows the results of microstructural characterization of the Ni–Ti sample after 3 passes of cold deformation. The EBSD method gives good support to the results of microscopic observations given in Fig. 4a. By indexing Kikuchi patterns from involved fcc and hcp phases, it allowed identifying both metallic components (Fig. 4b), as well as reconstruction of grain structure and crystallographic orientations inside particular Ni or Ti layers. In both cases, a typical for cold-rolled metals' lamellar structure was observed (Fig. 4c). On the other hand, the analysis carried out at higher magnifications revealed a substantial structural refinement inside layers represented also by a relatively high fraction of high angle grain boundaries (HAGBs) of ~40–47% (Fig. 4d). According to Hugh and Hansen [20], a presence of these structural features in deformed metals points towards an occurrence of local rotations of a crystal lattice that are necessary to accommodate plastic deformation in neighboring (micro)regions. Consequently, new highly misoriented boundaries having a “tilt-twist” character are produced.

Acquired EBSD data were also applied to examine microtexture evolution in Ni and Ti. Calculated ODFs were the microtexture was presented in  $\varphi_2 = 0, 45, 65^\circ$  and  $\varphi_2 = 0, 30, 60, 90^\circ$  sections (for Ni and Ti, respectively) of reduced Euler angles space ( $\varphi_1 = 0-90^\circ$ ,  $\Phi = 0-90^\circ$ ,  $\varphi_2 = 0-90^\circ$ ) (Fig. 5), as well as on pole figures (Fig. 6).

In general, the formation of a specific type of crystallographic texture during the cold rolling of fcc metals is determined by their stacking fault energy (SFE). Nickel is considered as high SFE ( $SFENi > 200 \text{ mJm}^{-2}$ ), and thus, it normally produces a so-called “pure metal”-type rolling texture [21]. This type of texture is characterized by well-developed Bs [22–24]  $\langle 211 \rangle$ ; S  $\{123\} \langle 634 \rangle$  and Cu  $\{221\} \langle 111 \rangle$  orientations having almost equally high intensities. In the present case, we can clearly distinguish ODF maxima at both Bs and S positions, but the Cu component is not observed, neither in the Euler Space (Fig. 5a) nor on pole figures (Fig. 6a). A lack of these orientations suggests that typical high SFE cross-slip of dislocations might be somehow suppressed, for example, when a high shear strain is imposed during the cold rolling process. An analogous textural evolution (related to destabilization and “disappearance” of Cu component) has been previously reported for pure Ni severely deformed by a differential speed rolling

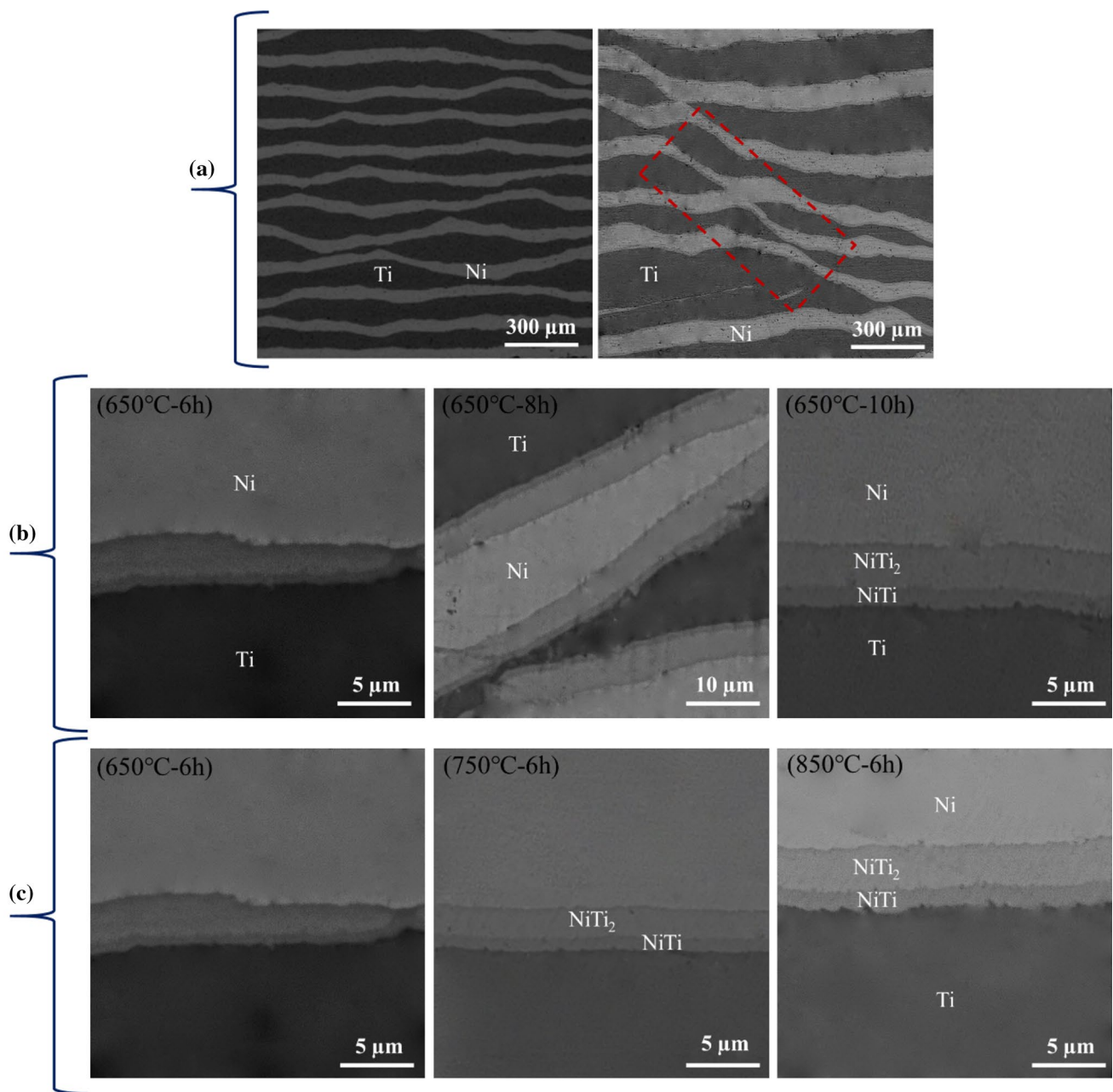


**Fig. 3** SEM images showing the samples: (a), before annealing (b), annealed 650 for 6, 8, and 10 h, and (c) annealed at 650, 750, and 850 for 6 h

method [25]. In the present work, the effect of shear straining is further confirmed by “blurring” and shifting primary Cube  $\{001\} \langle 100 \rangle$  orientations into positions corresponding to “Rotated Cubes” (denote as  $\{hkl\} \langle 100 \rangle$  and  $\{hkl\} \langle 110 \rangle$  in Fig. 5a, respectively) that have been recognized as shear texture components [26].

In the case of hcp metals, a type of crystallographic texture formed during cold deformation is mostly associated with the  $c/a$  ratio [27]. Titanium exhibits the  $c/a$  ratio of 1.588 which is below the ideal value of 1.633. In such a case, a  $\{0001\}$  basal texture is formed as the effect of

dislocation glide in  $\{0001\} \langle 110 \rangle$  principal slip system. Furthermore, as a consequence of deviation from the ideal  $c/a$  value, secondary slip systems might be activated, which is reflected in pole figures as tilting the basal poles. Indeed, in the present case, a strong  $\{0001\}$  basal texture is observed in both Euler space and pole figures (Figs. 5b and 6b). Furthermore, inspections of Euler space revealed a presence of  $\{010\}$  components corresponding to the prismatic slip system. Consequently, a combination of both slip systems results in tilting basal poles away from the normal direction, as it is observed in Fig. 6b.

**Fig. 4** The results of micro-structural characterization of ARBed-sample carried out on longitudinal sections (Normal Direction–Rolling Direction plane): a low magnification LM image (a); EBSD phase map showing a localization of Ni and Ti (b); high-magnification EBSD inverse pole figure maps for Ni (c) and Ti (d). Color code in (c) and (d) is consistent with basic triangles and black lines denote HAGBs

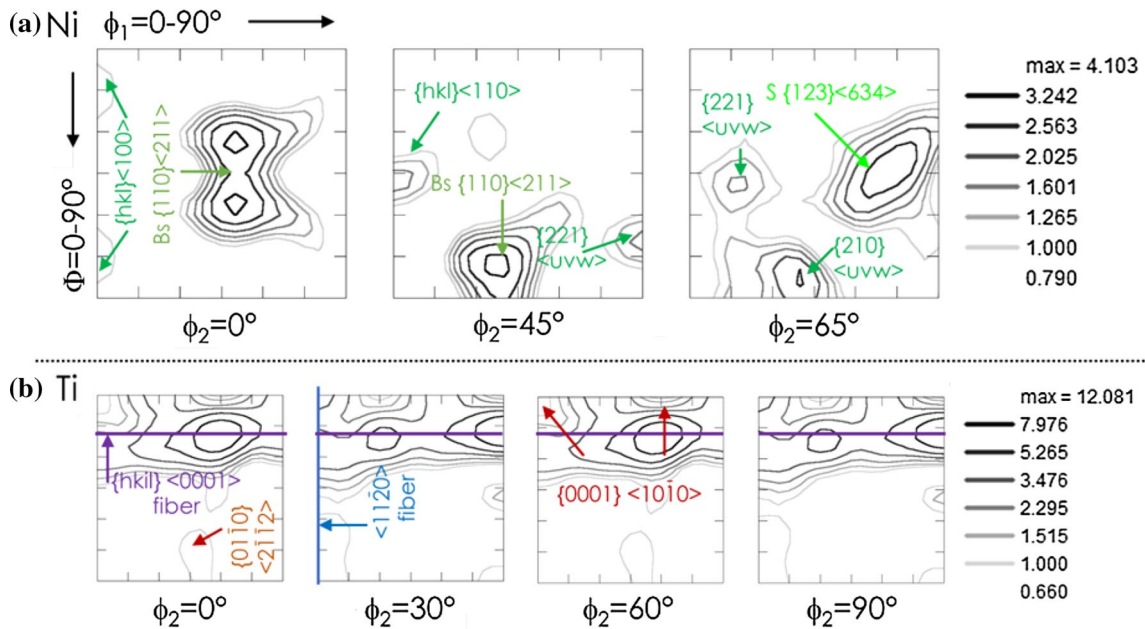
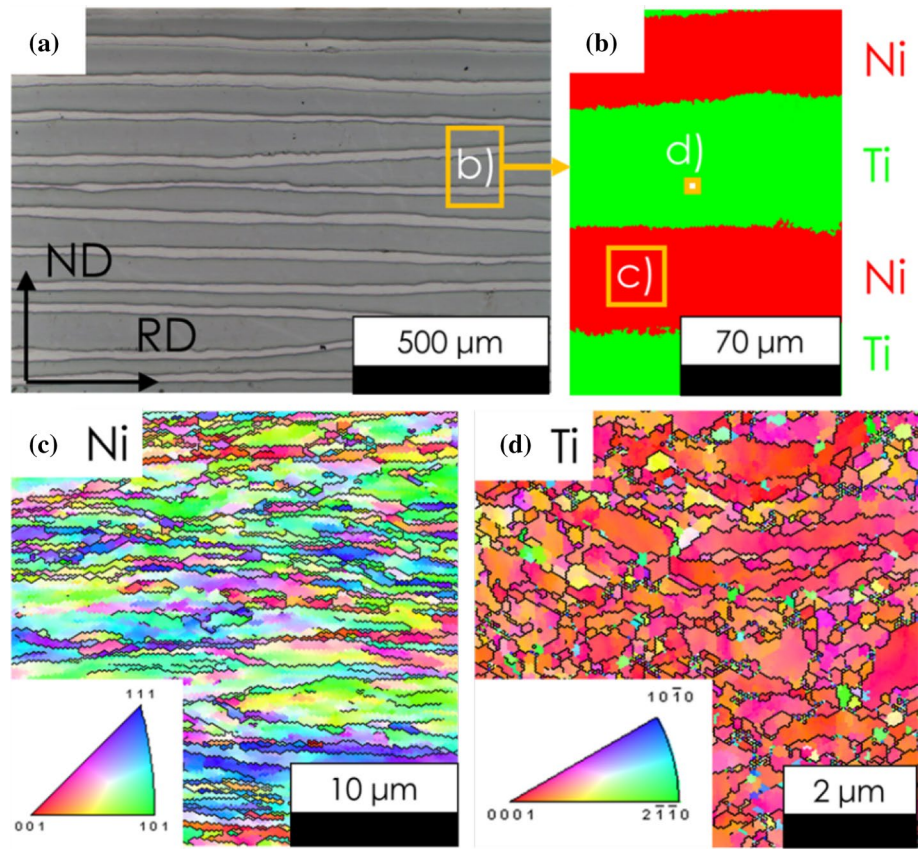


**Fig. 5** A crystallographic texture developed in the ARBed-sample represented as ODFs in selected sections of Euler angles space for Ni (a) and Ti (b)

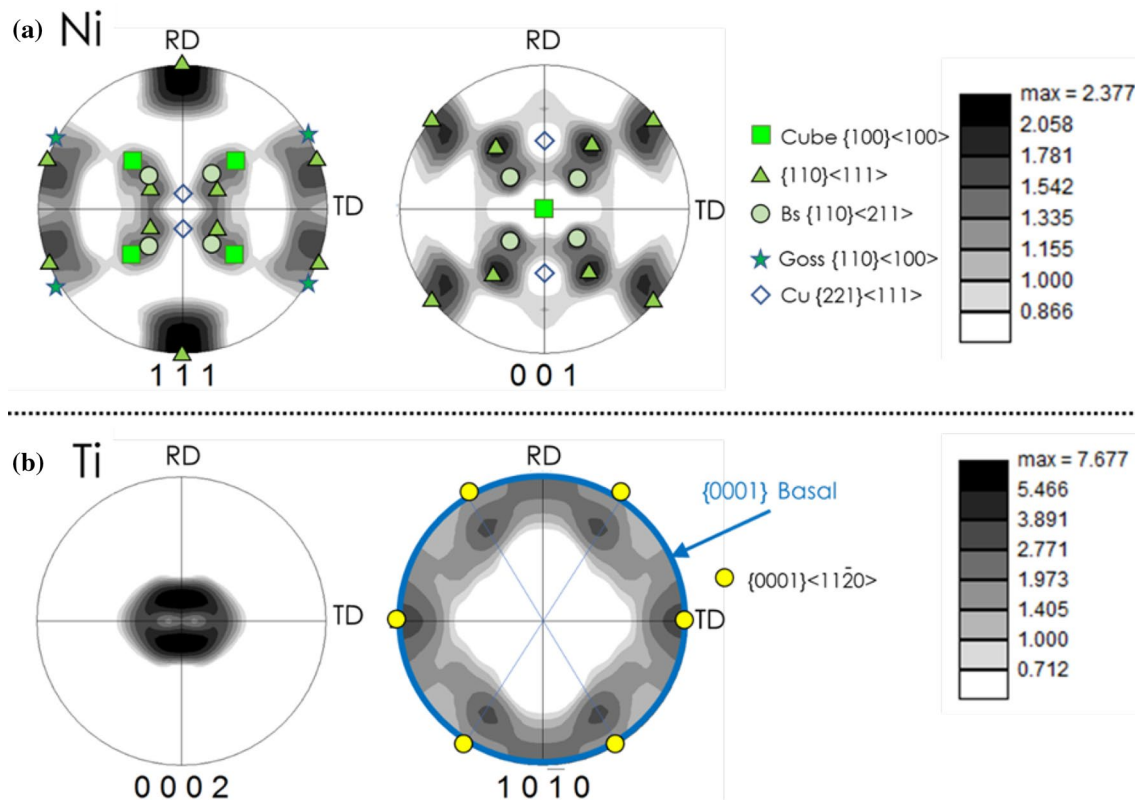


**Fig. 6** A crystallographic texture developed in the ARBed-sample represented as ODFs in pole figures for Ni (a) and Ti (b). RD and TD denote Rolling and Transverse Directions, respectively

### 3.2 Phase characterization and identification

Figure 3B and c displays the variation of interfacial layer thickness versus annealing temperatures and times. With an increase in the diffusion temperature and time, the thickness of the layers at Ni/Ti interfaces grew gradually. To analyze these layers, EDS and XRD analyses were performed on the cross section (ND-RD plane) of microstructures, as shown in Figs. 7 and 8. Based on XRD spectra of as-CARBed composite, there are no intermetallic compounds, and only Ti and Ni peaks can be seen. However, the XRD pattern of Ti/Ni laminated composite annealed at 850 °C for 6 h displays the peaks of Ti, Ni, TiNi, Ti<sub>2</sub>Ni, and TiNi<sub>3</sub>. Although there is a negligible amount of TiNi<sub>3</sub>, strong diffraction peaks of TiNi and Ti<sub>2</sub>Ni along with Ti and Ni peaks can be easily detected. EDS profile across diffusion zone reveals sharp changes of concentration of both elements between the layers as well as a fairly constant concentration of Ti and Ni on either side of the interfaces. The sharp changes indicate that there are distinctive interfaces across the composite. The constant concentrations represent the chemical compositions of two intermetallic phases including TiNi and Ti<sub>2</sub>Ni. Indeed, it can be inferred that annealing has a drastic effect on the interdiffusion of Ti and Ni atoms which then results

in the formation of intermetallic compounds at the interfaces [28–31].

It is generally accepted that TiNi, Ti<sub>2</sub>Ni, and TiNi<sub>3</sub> are the three main intermetallic phases in Ti–Ni binary system. Some researchers have studied the sequence of these phases at the Ti/Ni interfaces. Based on their reports, Gibbs free energy of formation and interfacial energy of intermetallic compounds play an important role in phase formation [29, 32]. Thermodynamically, TiNi<sub>3</sub> has the most negative Gibbs free energy of formation. It means that this phase is the most probable intermetallic phase to nucleate and grow at Ni/Ti interfaces. Also, it can be followed by Ti<sub>2</sub>Ni and TiNi. According to interfacial energy of phases, the formation of Ti<sub>2</sub>Ni, and TiNi<sub>3</sub> takes place prior to TiNi. Further, as stated by Bastin and Rieck, TiNi is unlikely to form before the nucleation and formation of Ti<sub>2</sub>Ni, and TiNi<sub>3</sub>. Therefore, according to XRD and EDS analyses, the nucleation of TiNi<sub>3</sub> takes place sooner than other phases during a shorter diffusion time. The growth of this phase may proceed till there is enough amount of Ti<sub>2</sub>Ni phase. In fact, the growth of Ti<sub>2</sub>Ni may hinder the growth of TiNi<sub>3</sub> or consume it. With an increase in diffusion time, TiNi nucleates and grows at TiNi<sub>3</sub>/Ti<sub>2</sub>Ni interface, as the thickness of Ti<sub>2</sub>Ni layer is expected to increase slowly. This is because the formation

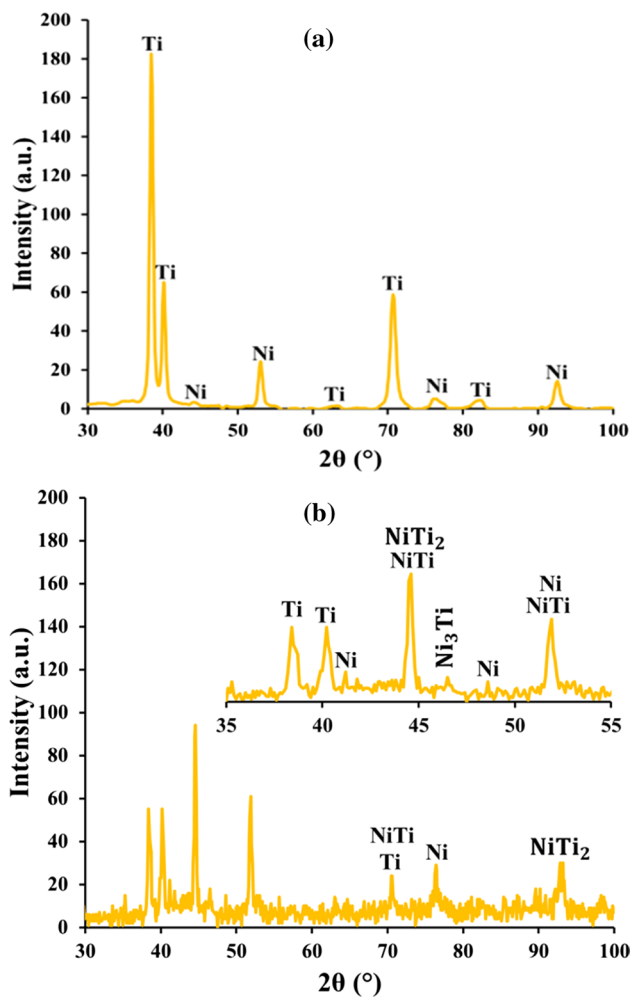


**Fig. 7** XRD patterns: **a** as-CARBed composite; **b** annealed composite at 850 °C for 6 h

of TiNi limits the diffusivity of Ni, thus decelerating the thickening of  $Ti_2Ni$  layer. Eventually, there is a thick layer of TiNi along with a relatively thin layer of  $Ti_2Ni$ , as can be observed in Fig. 3 (b) and (c).

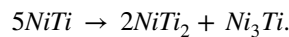
However, some other researchers believed that the diffusion of reactants through the layers is the driving force of reactions, and the probable reactions [33] and intermetallic can be in the following order:



According to the reactions above,  $Ni_3Ti$  nucleates after the other two phases at Ni/NiTi interface. However, this phase is not likely to grow significantly. This is certainly attributed to the hexagonal ( $a = 5.1 \text{ \AA}$ ,  $c = 8.3 \text{ \AA}$ ) structure

of  $NiTi_3$  which means that the third reaction may cause a strong change in crystal structure despite the fact that it is a thermodynamically favored phase [29, 32].

It is worthwhile mentioning that the following possible reaction may take place as a result of eutectoid transformation at 630 °C. Nonetheless, this reaction is neglected because of the temperature range of this paper



The thickness values of both  $Ti_2Ni$  and TiNi are listed in Table. At all annealing temperatures and times, the interfacial layers experienced a growth though the effect of annealing time was more significant. Taking into account that the formation of intermetallic phases consists of both lattice and grain boundary diffusion, the growth behavior of both intermetallic layers was evaluated by the following equation [7]:

$$X = kt^n$$

$$\ln x = \ln k + n \ln t.$$

In these equations,  $n$ ,  $x$ , and  $k$  are kinetic exponent, the thickness of an intermetallic layer, rate constant, and annealing time, respectively. The growth behavior is defined by the kinetic exponent. When  $n$  is 0.5 and 1, it represents the parabolic and linear behavior of growth kinetic (Table 1).

After substituting the values of thickness and diffusion time into Eq. 1, and applying linear regression, the kinetic exponents were achieved as listed in Table 2. The kinetics values indicate linear behavior for both intermetallic compounds. Nevertheless, as reported by some researchers, the growth of all phases is parabolic; therefore, the kinetic exponent is considered to be about 0.5 [29, 30]. This is because the nuclei of an intermetallic compound first form preferentially where there are dislocations and defects, and then, their growth occurs, indicating the existence of various sizes of grains within each intermetallic layer. Plus, it can be suggested that both lattice and grain boundary diffusion play a major role in the formation of intermetallic compounds [34, 35]; this is in good agreement with previously published papers [7]. From Table 1, it can be seen that, at annealing temperatures of 650 °C and 850 °C, the growth rate of TiNi is relatively higher than that of  $Ti_2Ni$ ; however, at 750 °C, the growth rate of both phases are quite the same. The marked growth is evident for TiNi at 850 °C and for  $Ti_2Ni$  at 750 °C when the samples were annealed for 10 h.

### 3.3 Mechanical analyses

Figure 9A and b shows the ultimate tensile strength and elongation under different annealing conditions. Evidently, the as-CARBed sample represented the highest strength and the lowest elongation. The annealed samples represented two



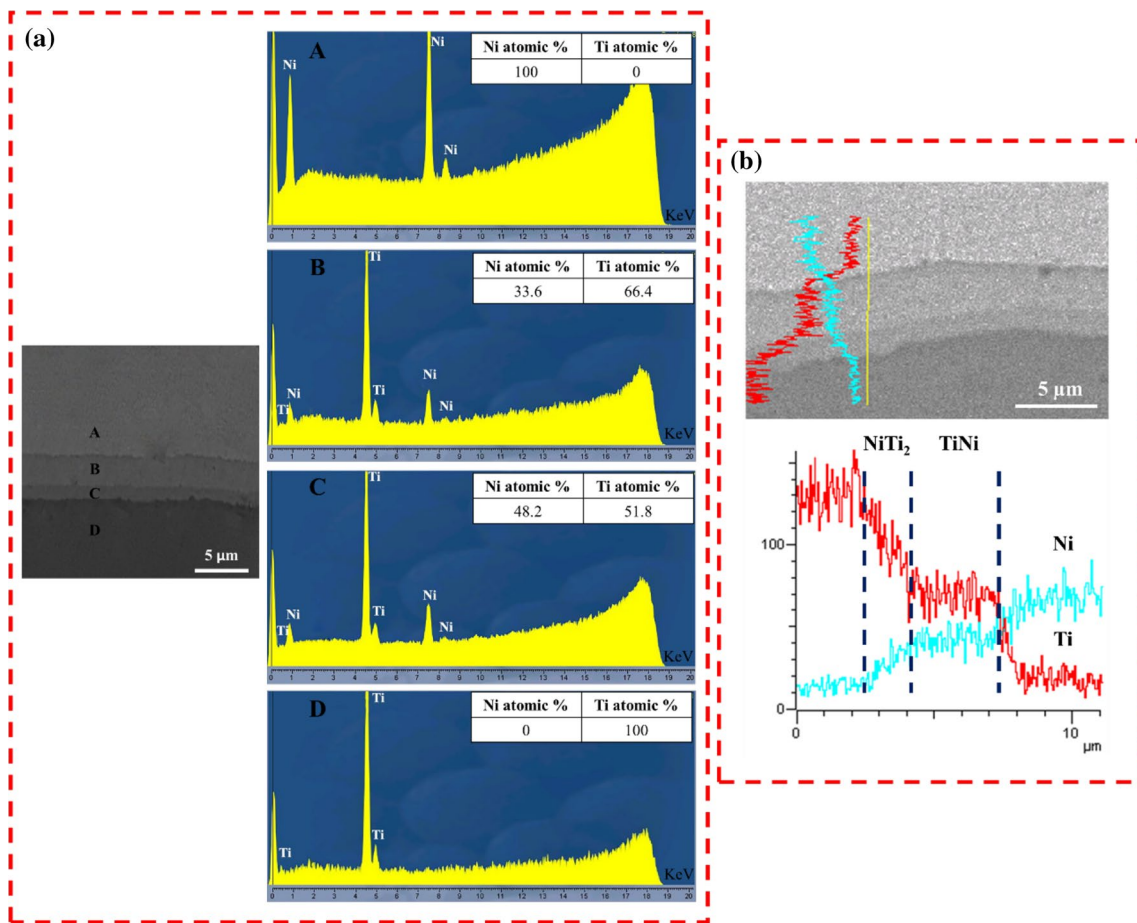


**Fig. 8** EDS analysis of interfacial layer of annealed sample: **a** 850 °C for 6 h and **b** 650 °C for 10 h

**Table 1** The measured values of intermetallic compounds at different times and temperatures (in micrometer)

Time (h)	Temperature (°C)			Time (h)	Temperature (°C)		
	650	750	850		650	750	850
6	0.7	2.1	2.7	<b>6</b>	2.1	5.2	5.4
8	1.1	2.5	3	<b>8</b>	3	5.5	5.8
10	1.2	4.1	4.7	<b>10</b>	3.5	5.6	8.4

Bold values indicate annealing time of NiTi intermetallic compound

**Table 2** Growth behavior, kinetics exponent, and activation energy of NiTi<sub>2</sub> and NiTi

Phases	Temperature (°C)	Kinetic exponent (n)	Growth behavior	Activation energy (kJ/mol)
NiTi	650	≈ 1	Linear growth	36.5
	750	≈ 0.5	Parabolic growth	
	850	≈ 1	Linear growth	
NiTi <sub>2</sub>	650	≈ 1	Linear growth	47
	750	≈ 1	Linear growth	
	850	≈ 1	Linear growth	

different trends. The ultimate strength showed a downward trajectory, while the elongation values fluctuated. These trends arise from layer softening during annealing treatment and the formation of brittle intermetallic layers. However, as can be seen, the samples annealed at 750 °C and 850 °C for 10 h have the lowest values of strength and elongation. These samples had the thickest interfacial layers. Therefore, the fracture of these samples may be caused by the fracture of brittle intermetallic layers due to the higher probability of crack initiation. Regarding the variation of elongation values, when the annealing temperature increased, three peaks

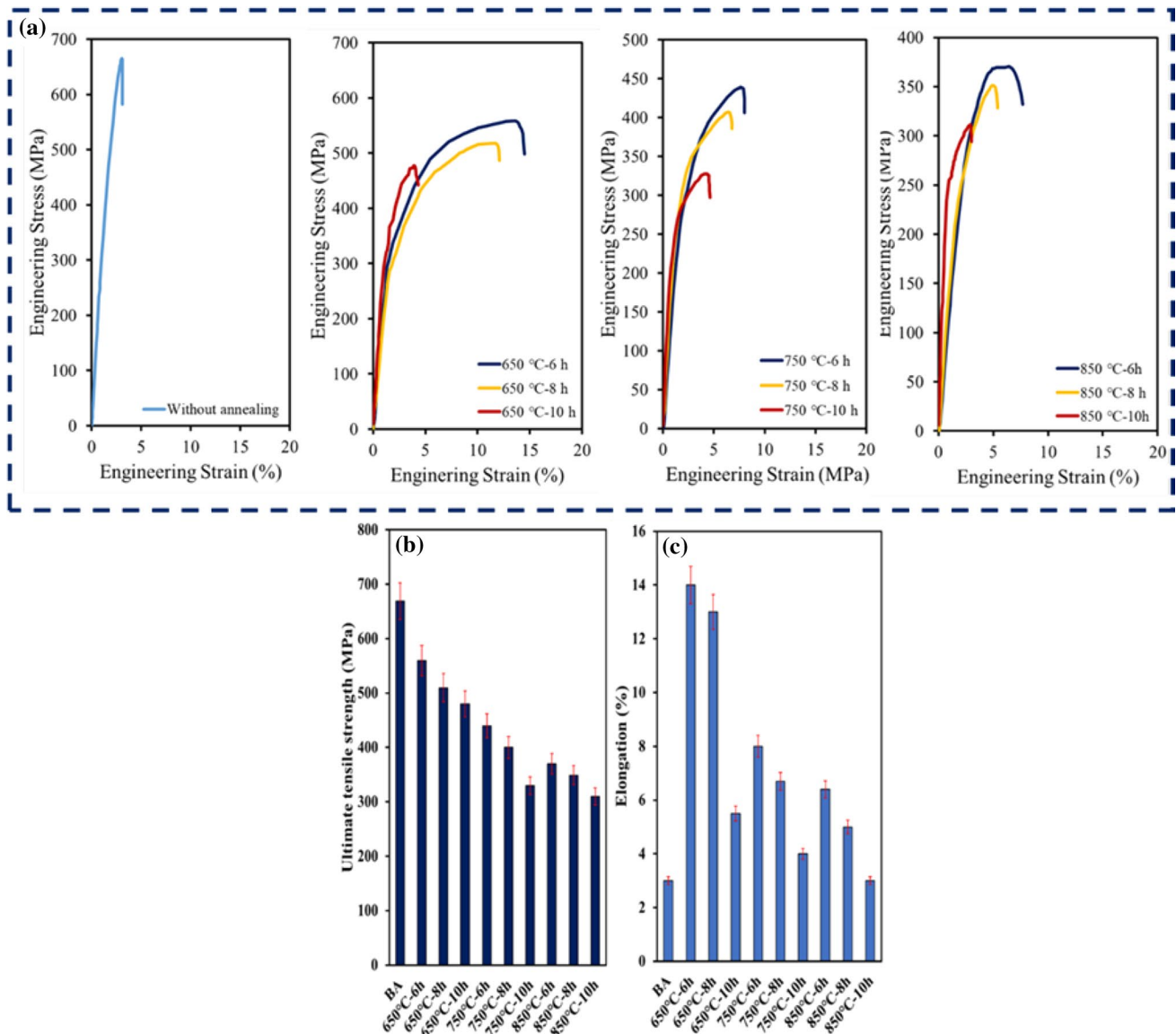


**Fig. 9** Tensile properties: **a** stress–strain curves [37], **b** ultimate strength, and **c** elongation

appeared as a result of softening. Then, as the samples were annealed for longer times, the values decreased gradually. In fact, annealing for 10 h produced a thicker interfacial layer which was very brittle.

Fracture surfaces, as shown in Fig. 10, show tearing ridges and many dimples on Ni and Ti layers, representing their ductile characteristics. Further, it can be seen the detachment of layers which is probably caused by the growth of intermetallic layers at the Ni/Ti interfaces; indeed, since the layers have different elastic moduli, there is a high probability of stress concentration and the separation of layers at interfaces [7]. Plus, cracks can often take place in both brittle intermetallic compounds, as shown in

Fig. 10b. It can be deduced that three reasons may contribute to fracture occurring in annealed laminated composites including a detachment of layers; ductile fracture of Ni and Ti layers; and cleavage fracture of NiTi and NiTi<sub>2</sub>. These findings are in good agreement with previously published papers [19]. Figure 11 which represent fracture surfaces on ND-RD plane also confirms ductile fracture of each layer and shows cracks propagation. It can be seen that intermetallic compounds can easily bridge the cracks' paths from one interface to the other one. In addition, comparing Fig. 11 b and c indicates that the formation of intermetallic facilitated the formation and propagation of cracks in laminated composite.

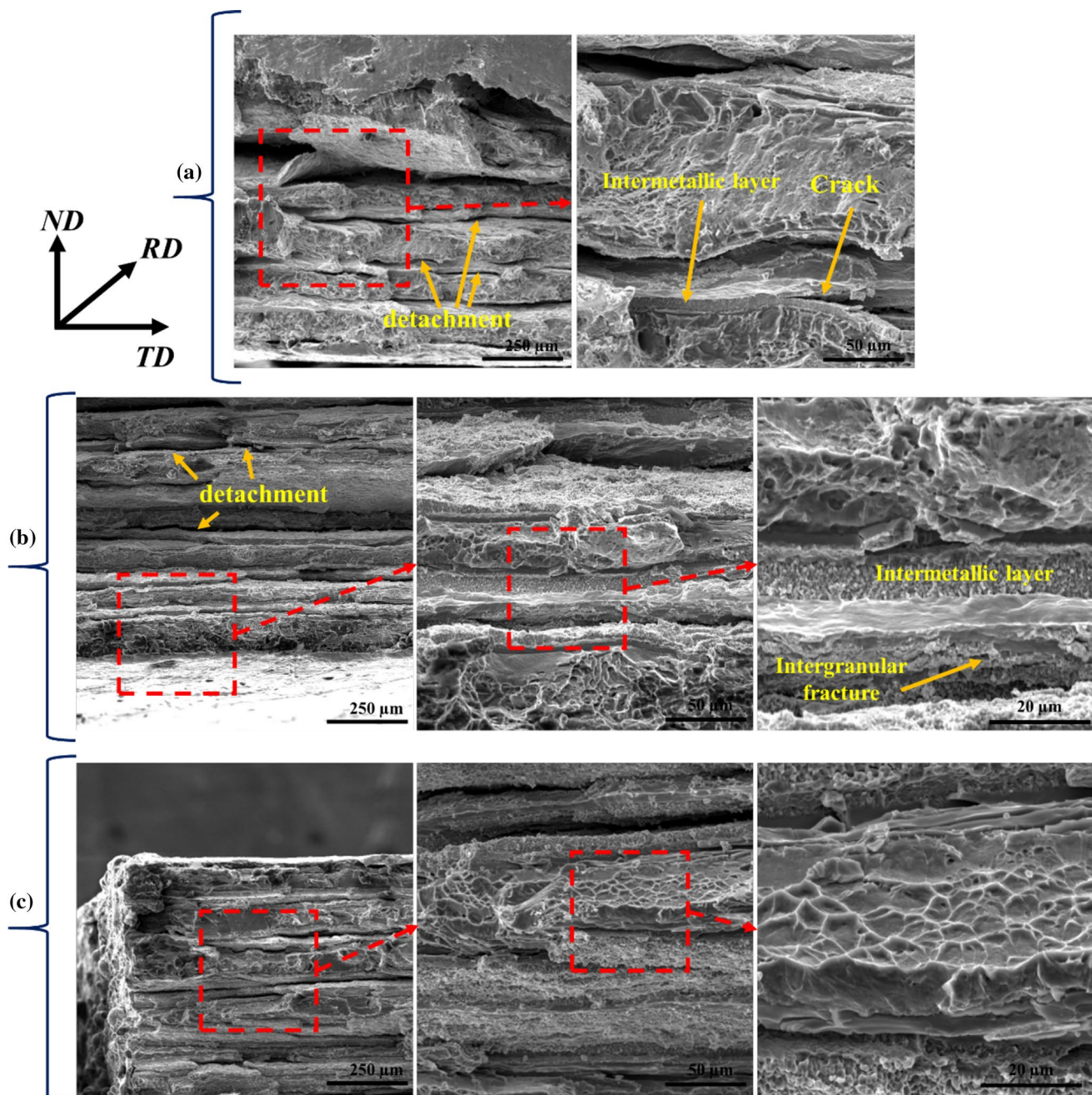


Fig. 10 SEM images showing the fracture surfaces of samples: **a** 650 °C, 6 h, **b** 750 °C, 6 h, and **c** 850 °C, 6 h

### 3.4 Wear properties

To compare the wear performance of samples at different loads, annealing temperatures, and, times, after performing the reciprocating pin-on-plate dry sliding wear test, the weight loss was accurately measured, as shown in Fig. 12. Clearly, there was a marked growth in the weight loss as the applied loads increased. However, by increasing the annealing temperatures and times, the weight loss declined slightly.

To evaluate the specific wear rate of samples, the following equation was used [19]:

$$w_r = \frac{\Delta m}{\rho L F_N}, \quad (4)$$

where  $w_r$ ,  $\Delta m$ ,  $\rho$ ,  $L$ , and  $F_N$  are usually defined as specific wear rate, wear mass loss, density, sliding distance, and normal force on the disk, respectively. The calculated wear rate is presented in Fig. 13. The wear resistance of samples rose

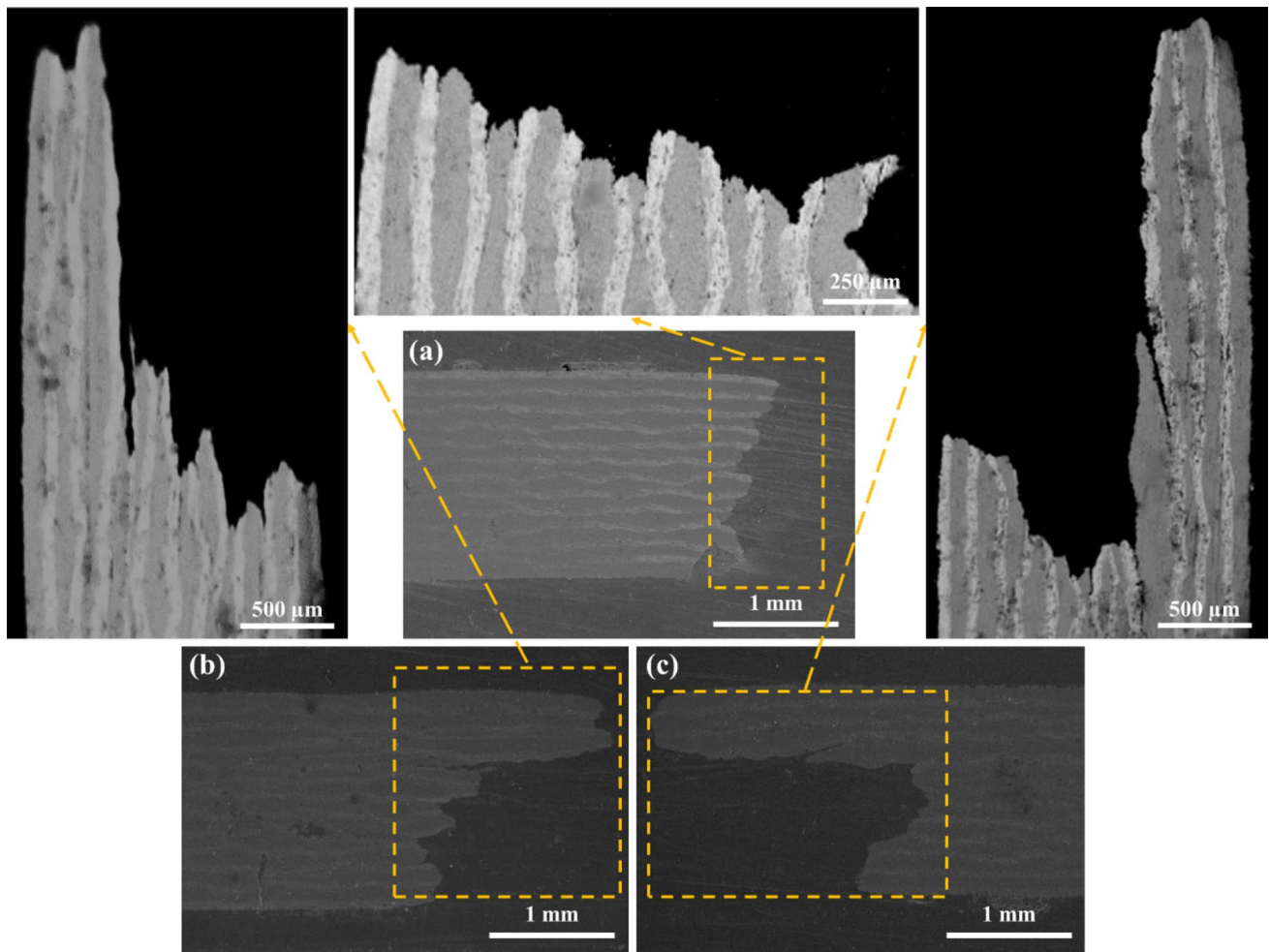


**Fig. 11** SEM images showing the cracks on fracture regions: **a** without annealing, **b** 650 °C, 6 h, and **c** 850 °C, 8 h

with an increase in annealing temperatures and times. It is believed that when the samples were annealed, their strength declined due to softening effect, as stated in a previously published paper [19]. This effect also may affect the wear rate. In fact, when the layers are hardened, they represent better wear resistance compared to annealed samples. In annealed samples softening effect is likely to increase the wear loss during the wear test. Nonetheless, the formation of intermetallic compounds acts adversely. It is believed that the composite becomes more resistant to wear as the thickness of intermetallic compounds grows at the interface of Ni/Ti as the temperature and time of annealing increases. In addition, it is well known that the formation of solid solution and intermetallic phases decreased the wear rate [36].

Figure 14 displays the friction coefficient of Ni/Ti composites at different wear loads, annealing temperatures, and times. As expected, with an increase in wear loads, steel pin can abrade the depth of composite which may involve more layers. However, Fig. 14 confirms that composites with higher amounts of intermetallic compounds at

higher temperatures and particularly longer times resulted in lower values of friction coefficient. In fact, the higher hardness of intermetallic compounds brought about the easier movement of steel pin on composites [36]. Since the number of interfaces was the same and the intermetallic layers formed relatively uniformly across the composite, the friction coefficient fluctuates repeatedly with an increase in sliding distance.

Figures 15 shows the profilometry of wear tracks under two loads and annealing times. Comparing the curves in figure a indicates that material removal from plates increased by increasing loads but decreased by annealing times. As mentioned earlier, the latter can be attributed to softening effect. In fact, wear loss at higher times and temperatures experienced a decline on account of the increased thickness of intermetallic compounds formed at Ni/Ti interfaces. This growth led to little removal of worn surfaces. This in agreement with previously published paper (ref).

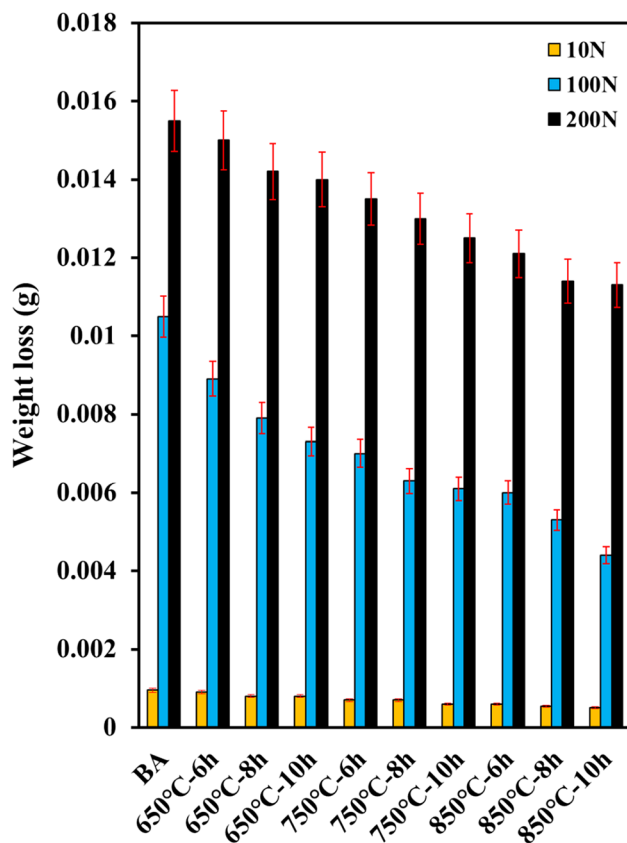


Fig. 12 Weight loss at different annealing times and temperatures

### 3.5 Characterization of worn surfaces

Figures 16, 17, 18, 19, 20 display the worn surfaces of Ni/Ti laminated composite at different annealing temperatures, times, and wear loads. Evidently, there are several wear mechanisms on these surfaces. When steel pin and composite plate come into contact, as a result of adhesion and plowing, normal and tangential loads are concentrated at contact loads. Then, the asperities of plate surfaces become deformed or fractured because of the steel pin sliding on plate. The hard asperities of pin during cyclic loading can easily plow the surface of the plate that often pulls out particles from surface, as shown at magnification in figure. Also, the plowing effect leads to accumulation of plastic shear deformation which in turn cause crack propagation below the surface, as can be seen in Fig. 20. Any further deformation during repeated wear loads may cause crack propagation. Cracks often propagate to join the adjacent ones. The growth of the subsurface cracks then can result in delamination. Alternatively, when cracks shear the surface, wear debris are generated. It is generally believed that the undersides of these debris are opposite the sliding direction, as shown in Figs. 16, 17, 18.

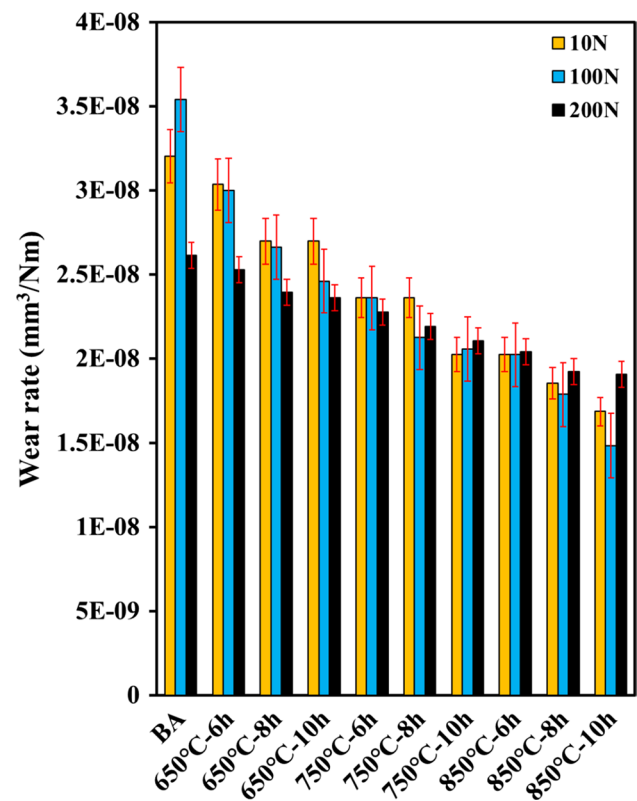
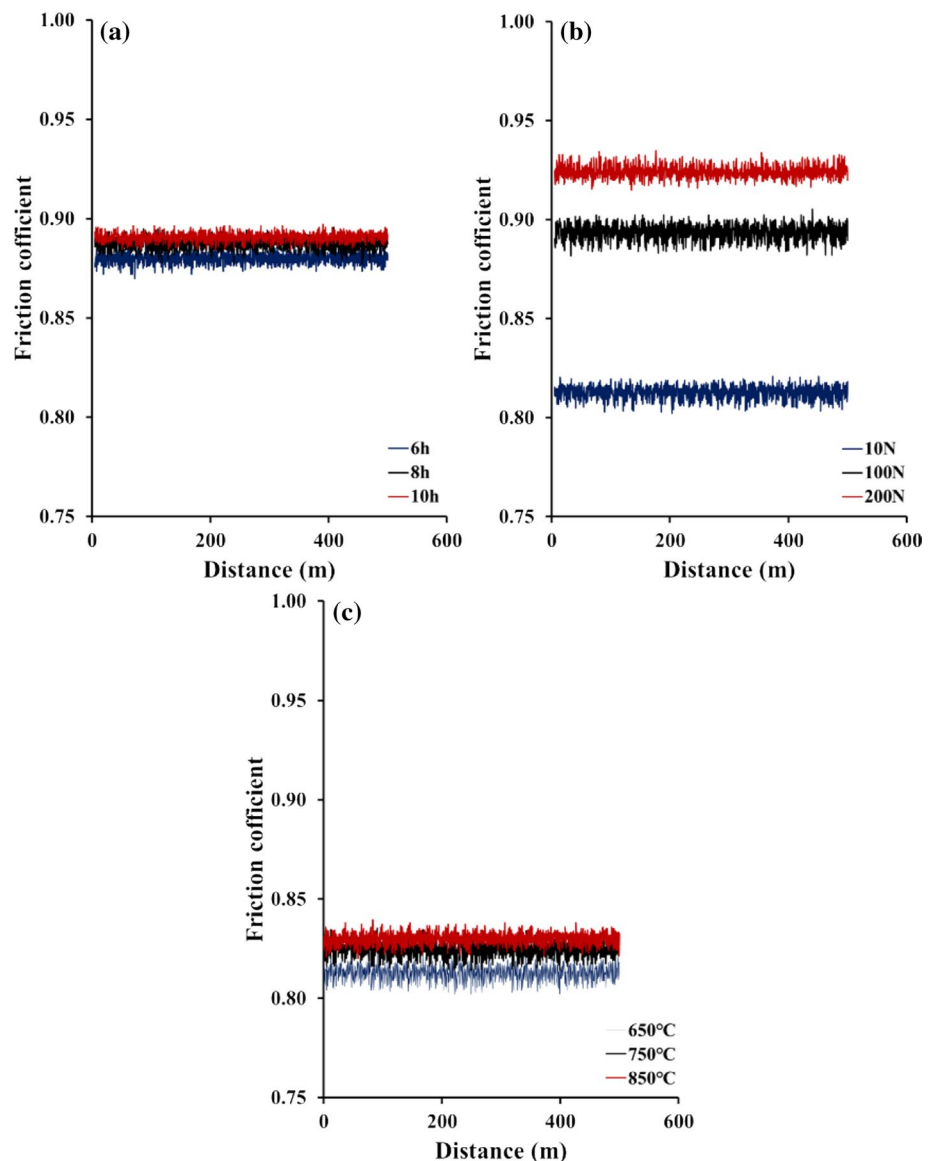


Fig. 13 Wear rate at different annealing times and temperatures

At higher wear loads, during the sliding of hard pin on soft plate, the particles which are pulled out promote the abrasion, as can be seen in figure. However, at higher annealing temperature and times when higher amounts of intermetallic compounds at Ni/Ti interfaces exist, repeated reciprocating sliding can abrade the depth of composite plate. Nevertheless, when slider reach the ceramic layer, wear loss decreases. This is because intermetallic layers possess higher hardness which decelerate the wear process. As can be seen in Figs. 17 and 18, the sample without annealing treatment represents noticeable grooves in comparison to the annealed samples. This difference is certainly attributed to the growth of intermetallic compounds which enhance the wear resistance of composites. These findings are in good agreement with previously published paper in which adhesion, abrasion, and delamination were observed on worn surfaces [19].

It is generally believed that the mechanical properties of materials such as hardness, toughness, and tensile strength have an impact on their wear resistance [16]. As reported in the previously published paper, the weight loss decreased as the values of hardness pertaining to Al/Ti/Steel composite rose [19]. It can be inferred that as a result of intermetallic formation, composites become more resistant to wear. Therefore, as shown in Fig. 17, by increasing annealing time, the plowing

**Fig. 14** Friction coefficients at different: **a** times, **b** loads, and **c** temperature



effect cannot lead to deep grooves; indeed, the wear resistance of intermetallic is much more than Ni and Ti layers. Moreover, at higher magnifications, adhesive debris particles can be clearly seen, especially at higher loads. EDS results in Fig. 21 also showed that layers were abraded at higher loads. Thus, as a result of intermetallic formation, three wear mechanisms were detected in this research including adhesive, abrasive, and delamination mechanisms both of which were more evident at higher wear loads, temperatures, and shorter times (Fig. 18).

## 4 Conclusions

This paper has investigated the fabrication of Ni/Ti laminated composite using the CARB process and annealing treatment. Effects of different annealing times and

temperatures on microstructure, wear, and mechanical properties have been examined, and the main results have been summarized below:

1. Applying severe plastic deformation by ARB process led to good bonding of interfaces without detachment and voids, although nickel layers experienced instabilities.
2. According to EBSD analyses, lamellar structure was observed on samples. Furthermore, at higher magnifications, a relatively high fraction of high angle grain boundaries indicated the substantial structural refinement inside layers. Applying severe plastic deformation led to formation of highly misoriented boundaries. Also, on nickel layer, the shear texture was confirmed by blurring and shifting of primary Cube {001} <100> orientations into positions corresponding to Rotated Cubes. On

**Fig. 15** Profilometry of wear tracks: **a** under 100 N annealed at 850 °C for 6 h and 8 h, and **b** under 100 and 200 N annealed at 750 °C 10 h

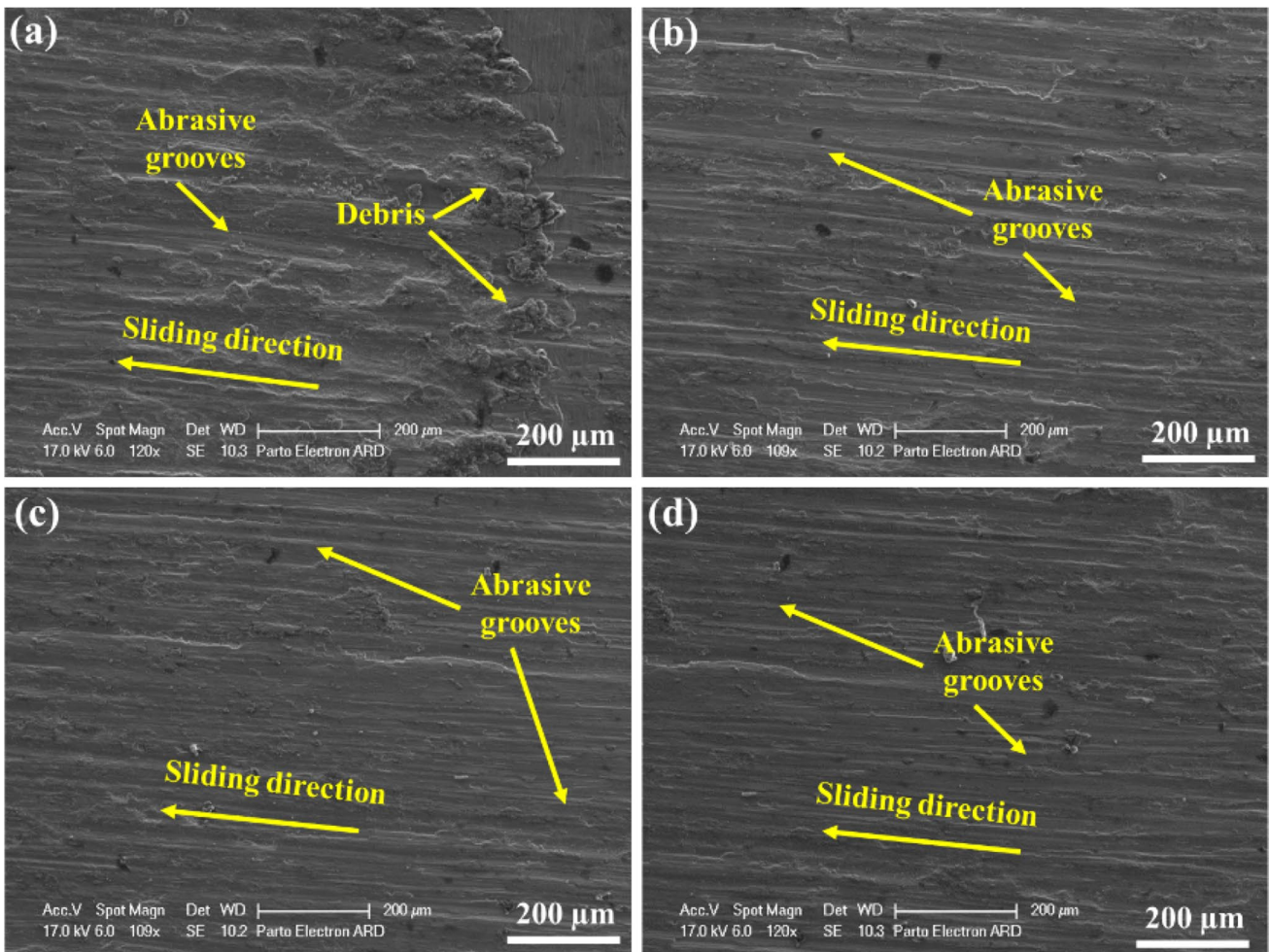
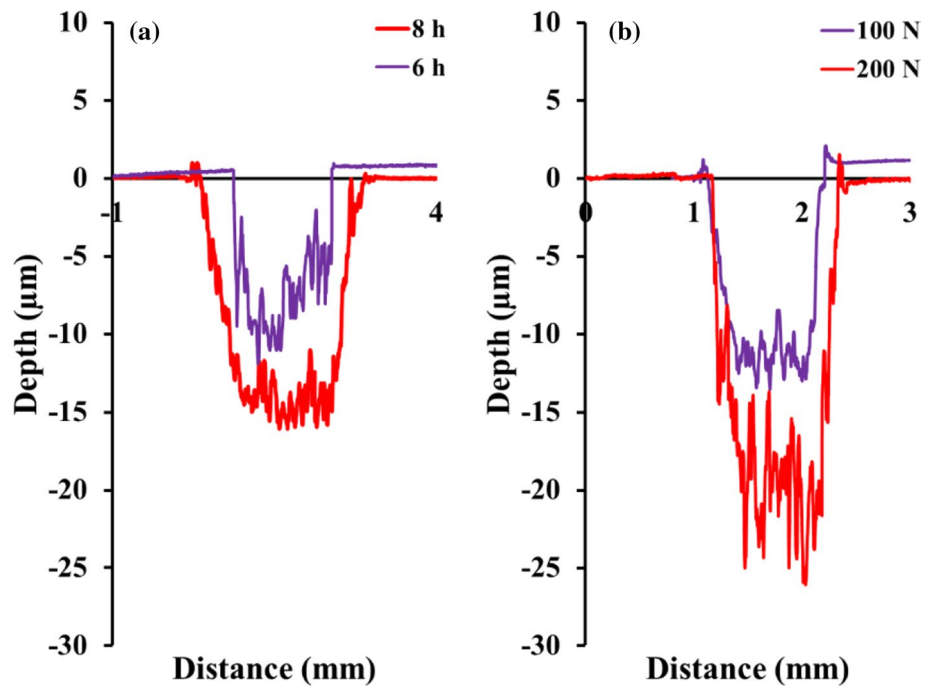


**Fig. 16** SEM images showing worn surfaces under 200 N: **a** without annealing, **b** 650 °C, 8 h, **c** 750 °C, 8 h, and **d** 850 °C, 8 h

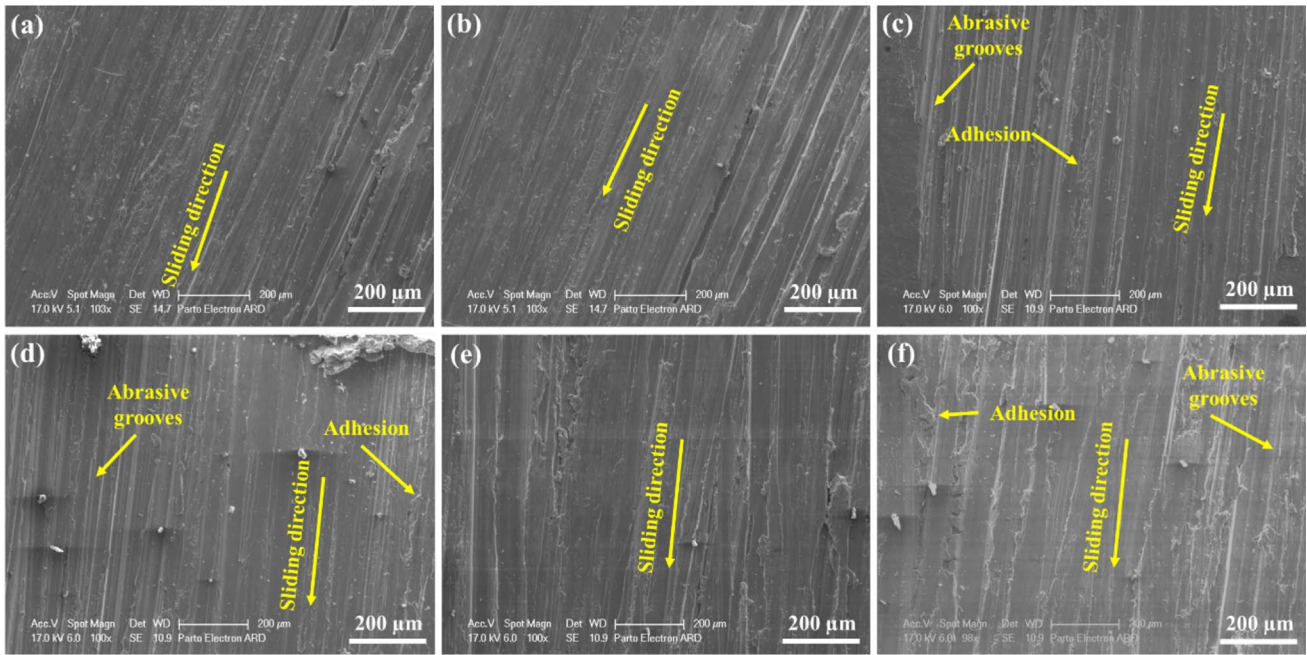


**Fig. 17** SEM images showing worn surface annealed: **a** 6 h, **b** 8 h, and **c** 10 h at 650 °C, under wear load of 200 N, **d** 850 °C, **e** 750 °C, and **f** 650 °C for 8 h under wear load of 100 N

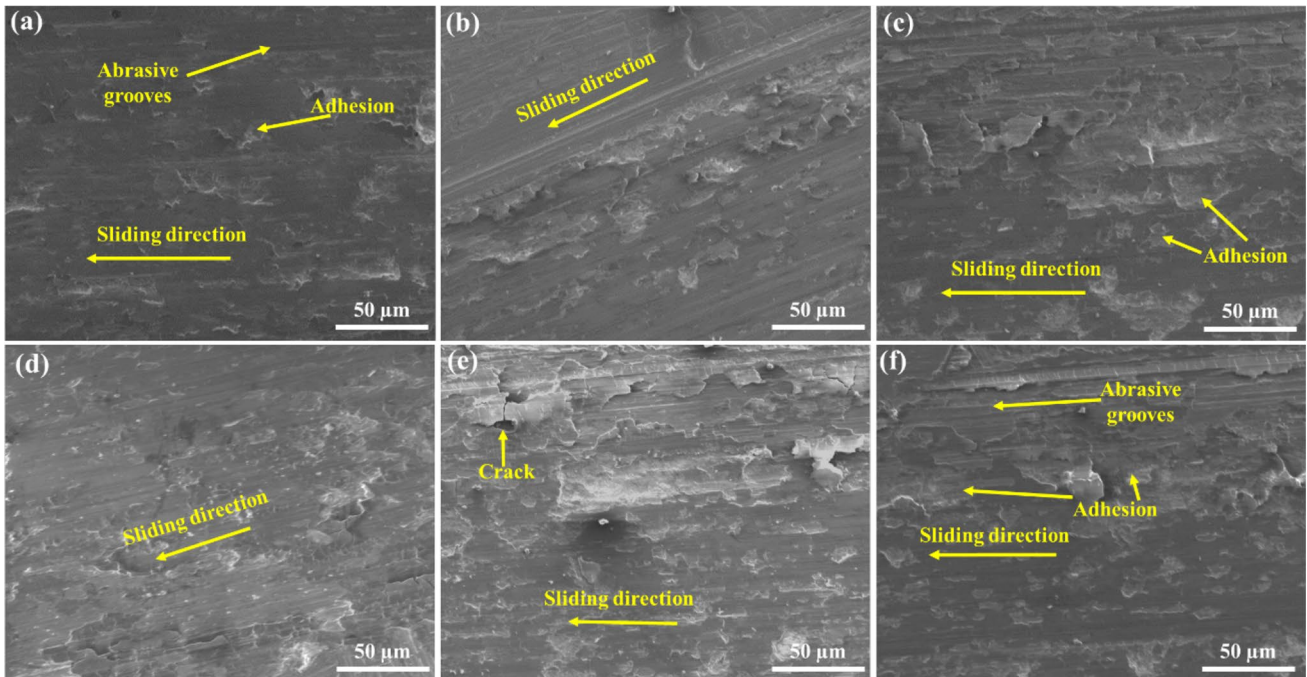


**Fig. 18** SEM images showing worn surfaces annealed at: 750 °C for 4 h under wear loads of **a** 10 N, **b** 100 N, and **c** 200 N; annealed at 650 °C for 4 h under wear load of **d** 10 N, **e** 100 N, and **f** 200 N

the other hand, on titanium layer, tilting of basal poles away from the normal direction indicated the crystallographic texture formed during three passes of roll bonding.

3. SEM images demonstrated that interfaces did not show the formation of oxides at high temperatures because of the encapsulation of samples in quartz tubes. Also, EDS analysis revealed that annealing treatment caused three



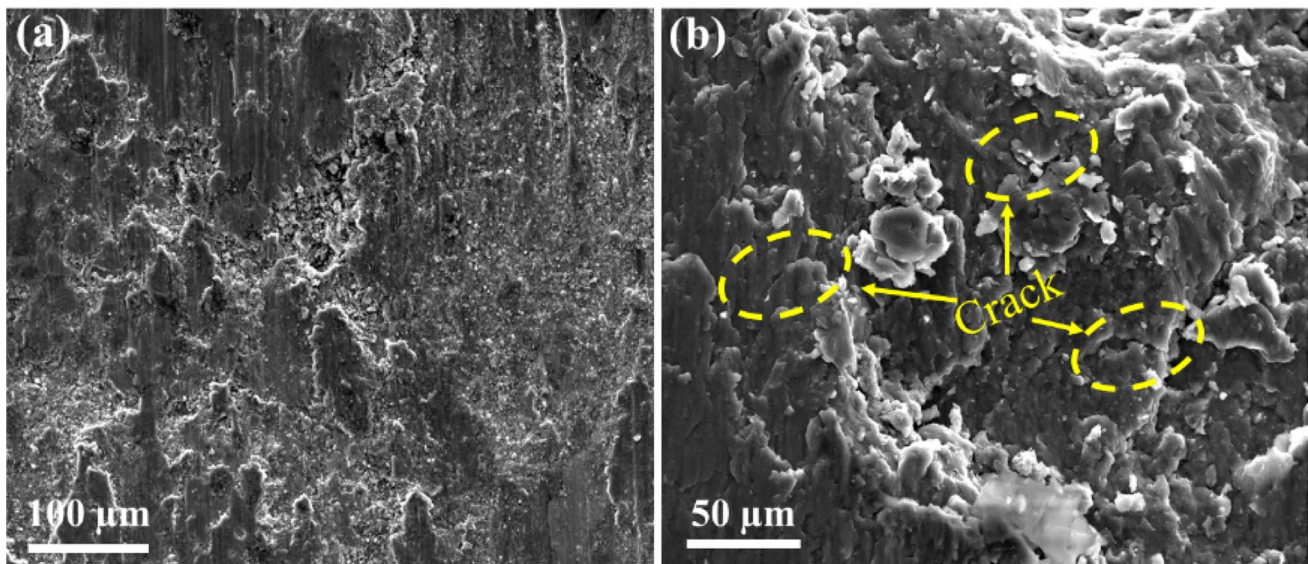


**Fig. 19** Debris on worn surfaces of sample annealed at 750 °C for 8 h at different magnifications

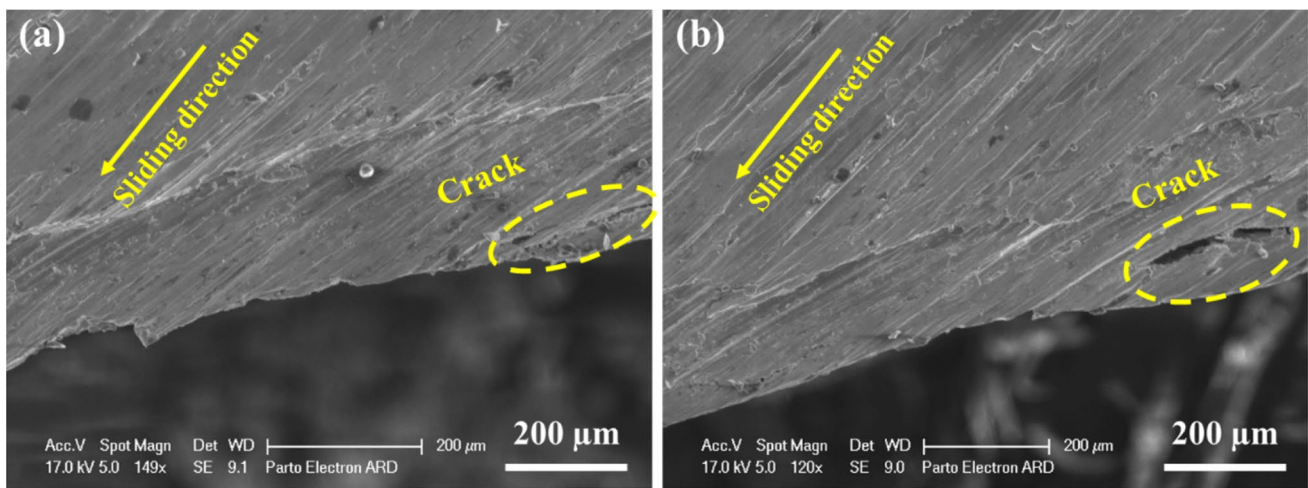


**Fig. 20** Section view (on ND-TD plane) of worn surfaces of sample annealed at 650 °C for 6 h under 200 N

intermetallic phases to emerge; nevertheless, NiTi and NiTi<sub>2</sub> were dominant.

4. As intermetallic layers grew, the ultimate strength declined, but elongation fluctuated. The fluctuation was caused by softening and thickening of brittle intermetallic layers.
5. The results of wear tests indicated that in spite of softening effect during annealing treatment, the wear resistance of composites increased by increasing times and temperatures on account of intermetallic layers including NiTi and NiTi<sub>2</sub>. In addition, cracks were observed under worn surfaces caused by the accumulation of plastic shear deformation due to plowing effect.
6. The friction coefficients of composite experienced a decrease since intermetallic compounds with higher hardness than Ni and Ti layers led to the easier movement of steel pin on composites.
7. According to profilometry analyses on wear tracks, the material removal from plates increased by increasing loads. However, with an increase in annealing times, less material was removed on account of the increased thickness of intermetallic compounds at Ni/Ti interfaces.

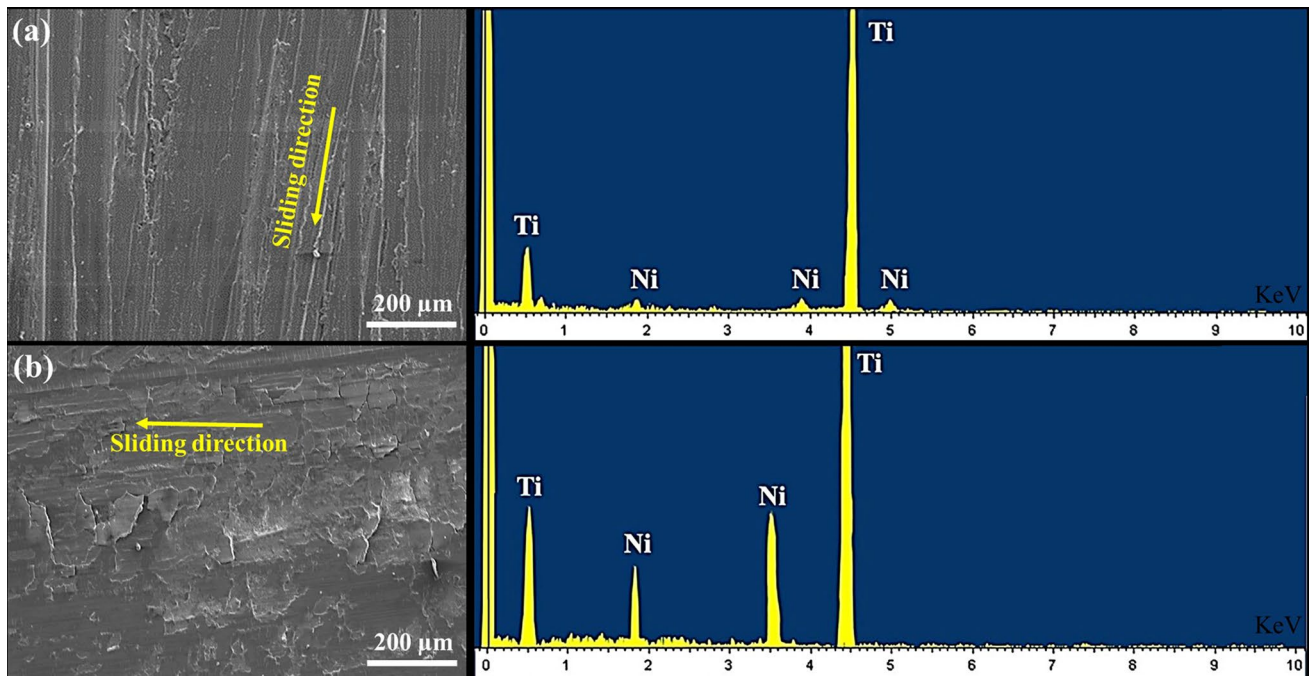


**Fig. 21** EDS analysis on worn surfaces: **a** 750 °C, 4 h, 100 N, and **b** 750 °C, 4 h, 200 N

**Funding** This research received no specific grant.

## Declarations

**Conflict of interest** The authors declare that they have no conflict of interest.

**Ethical approval** All procedures performed in studies involving human participants were in accordance with the ethical standards of the institutional and/or national research committee and with the 1964 Helsinki declaration and its later amendments or comparable ethical standards.

## References

- Bai Y, Nardi DC, Zhou X, Picon RA, Florez-Lopez J. A new comprehensive model of damage for flexural subassemblies prone to fatigue. *Comput Struct*. 2021;256:106639.
- Cui W, Li X, Li X, Si T, Lu L, Ma T, et al. Thermal performance of modified melamine foam/graphene/paraffin wax composite phase change materials for solar-thermal energy conversion and storage. *J Clean Prod*. 2022;367:133031.
- Gao T, Li C, Wang Y, Liu X, An Q, Li HN, et al. Carbon fiber reinforced polymer in drilling: from damage mechanisms to suppression. *Compos Struct*. 2022;286:115232.
- Gurau G, Gurau C, Fernandes FMB, Alexandru P, Sampath V, Marin M, et al. Structural characteristics of multilayered Ni-Ti nanocomposite fabricated by high speed high pressure torsion (HSHT). *Metals*. 2020;10(12):1629.
- Liang L, Xu M, Chen Y, Zhang T, Tong W, Liu H, et al. Effect of welding thermal treatment on the microstructure and mechanical properties of nickel-based superalloy fabricated by selective laser melting. *Mater Sci Eng, A*. 2021;819:141507.
- Zhong Y, Xie J, Chen Y, Yin L, He P, Lu W. Microstructure and mechanical properties of micro laser welding NiTiNb/Ti6Al4V dissimilar alloys lap joints with nickel interlayer. *Mater Lett*. 2022;306:130896.
- Assari AH, Eghbali B. Solid state diffusion bonding characteristics at the interfaces of Ti and Al layers. *J Alloy Compd*. 2019;773:50–8.
- Fronczek D, Chulist R, Szulc Z, Wojewoda-Budka J. Growth kinetics of TiAl<sub>3</sub> phase in annealed Al/Ti/Al explosively welded clads. *Mater Lett*. 2017;198:160–3.
- Huang J, Tayyebi M, Assari AH. Effect of SiC particle size and severe deformation on mechanical properties and thermal conductivity of Cu/Al/Ni/SiC composite fabricated by ARB process. *J Manuf Process*. 2021;68:57–68.
- Tayyebi M, Eghbali B. Microstructure and mechanical properties of SiC-particle-strengthening tri-metal Al/Cu/Ni composite produced by accumulative roll bonding process. *Int J Miner Metall Mater*. 2018;25(3):357–64.
- Tayyebi M, Rahmatabadi D, Karimi A, Adhmi M, Hashemi R. Investigation of annealing treatment on the interfacial and mechanical properties of Al5052/Cu multilayered composites subjected to ARB process. *J Alloy Compd*. 2021;871:159513.
- Shi J, Cao Z, Wei M, Pan G, Xu L, Meng X. Anomalous softening behavior in Ti/Ni multilayers with ultra-high hardness. *Mater Sci Eng, A*. 2014;618:385–8.
- Ding H-S, Lee J-M, Lee B-R, Kang S-B, Nam T-H. Effects of subsequent heat treatment on the shape memory behaviors of a Ti/Ni sheet fabricated by bonding and cold rolling of Ti/Ni multilayers. *Mater Sci Eng, A*. 2007;444(1–2):265–70.
- Zhang Y, Cheng X, Cai H, Zhou S, Wang P, Yin J. The effects of thickness of original Ti foils on the microstructures and

- mechanical properties of Ti2Ni/TiNi laminated composites. *Mater Sci Eng, A*. 2017;684:292–302.
15. Khosravi G, Sohi MH, Ghasemi H, Karazmoudeh NJ. 2021 Comparative tribological study of NiTi diffusion coated titanium with pure titanium.
  16. Wachowski M, Zygmuntowicz J, Kosturek R, Konopka K, Kaszura W. Manufacturing of Al<sub>2</sub>O<sub>3</sub>/Ni/Ti composites enhanced by intermetallic phases. *Materials*. 2021;14(13):3510.
  17. Avazzadeh M, Alizadeh M, Tayyebi M. Structural, mechanical and corrosion evaluations of Cu/Zn/Al multilayered composites subjected to CARB process. *J Alloy Compd*. 2021;867:158973.
  18. Merriman C, Field D, Trivedi P. Orientation dependence of dislocation structure evolution during cold rolling of aluminum. *Mater Sci Eng, A*. 2008;494(1–2):28–35.
  19. Wang Y, Tayyebi M, Assari A. Fracture toughness, wear, and microstructure properties of aluminum/titanium/steel multi-laminated composites produced by cross-accumulative roll-bonding process. *Archiv Civil Mech Eng*. 2022;22(1):1–14.
  20. Hughes DA, Hansen N. Microstructure and strength of nickel at large strains. *Acta Mater*. 2000;48(11):2985–3004.
  21. Polkowski W, Józwiak P, Karczewski K, Bojar Z. Evolution of crystallographic texture and strain in a fine-grained Ni3Al (Zr, B) intermetallic alloy during cold rolling. *Archiv Civil Mech Eng*. 2014;14(4):550–60.
  22. Zeng L, Gao R, Fang Q, Wang X, Xie Z, Miao S, et al. High strength and thermal stability of bulk Cu/Ta nanolamellar multilayers fabricated by cross accumulative roll bonding. *Acta Mater*. 2016;110:341–51.
  23. Zhang Y, Li C, Jia D, Zhang D, Zhang X. Experimental evaluation of the lubrication performance of MoS<sub>2</sub>/CNT nanofluid for minimal quantity lubrication in Ni-based alloy grinding. *Int J Mach Tools Manuf*. 2015;99:19–33.
  24. Zhao Y, Liu K, Hou H, Chen L-Q. Role of interfacial energy anisotropy in dendrite orientation in Al-Zn alloys: A phase field study. *Mater Design*. 2022;216:110555.
  25. Polkowski W, Polkowska A, Zasada D. Characterization of high strength nickel thin sheets fabricated by differential speed rolling method. *Mater Charact*. 2017;130:173–80.
  26. Simoes FJ, de Sousa RJA, Gracio JJ, Barlat F, Yoon JW. Mechanical behavior of an asymmetrically rolled and annealed 1050-O sheet. *Int J Mech Sci*. 2008;50(9):1372–80.
  27. Wang Y, Huang J. Texture analysis in hexagonal materials. *Mater Chem Phys*. 2003;81(1):11–26.
  28. Milosavljević M, Toprek D, Obradović M, Grce A, Peruško D, Dražić G, et al. Ion irradiation induced solid-state amorphous reaction in Ni/Ti multilayers. *Appl Surf Sci*. 2013;268:516–23.
  29. Zhang C, Liu W. Non-parabolic Al<sub>3</sub>Ti intermetallic layer growth on aluminum-titanium interface at low annealing temperatures. *Mater Lett*. 2019;256:126624.
  30. Zhang C, Liu W. Abnormal effect of temperature on intermetallic compound layer growth at aluminum-titanium interface: the role of grain boundary diffusion. *Mater Lett*. 2019;254:1–4.
  31. Zhang C, Robson JD, Haigh SJ, Prangnell PB. Interfacial segregation of alloying elements during dissimilar ultrasonic welding of AA6111 aluminum and Ti6Al4V titanium. *Metall Mater Trans A*. 2019;50(11):5143–52.
  32. Gao Q, Wang W, Yi G, Wang B, Feng X, Shi P, et al. High temperature and room temperature tribological behaviors of in-situ carbides reinforced Ni-based composites by reactive sintering Ni and Ti<sub>2</sub>AlC precursor. *Wear*. 2022;488:204165.
  33. Zhang B, Zhang Z, Zhao T, Zhang D, Cheng J, Wang W, et al. Effect of temperature on the interfacial evolution of Ti/Ni multi-layered composites fabricated by ARB. *J Alloy Compd*. 2019;803:265–76.
  34. Assari A, Eghbali B. Interfacial layers evolution during annealing in Ti-Al multi-laminated composite processed using hot press and roll bonding. *Met Mater Int*. 2016;22(5):915–23.
  35. Tayyebi M, Alizadeh M. A novel two-step method for producing Al/Cu functionally graded metal matrix composite. *J Alloy Compd*. 2022;911:165078.
  36. Akbarpour M, Alipour S, Najafi M, Ebadzadeh T, Kim H. Microstructural characterization and enhanced hardness of nanostructured Ni<sub>3</sub>Ti–NiTi (B2) intermetallic alloy produced by mechanical alloying and fast microwave-assisted sintering process. *Intermetallics*. 2021;131:107119.
  37. Luo J, Yarigarravesh M, Assari AH, Amin NH, Tayyebi M, Paidar M. Investigating the solid-state diffusion at the interface of Ni/Ti laminated composite. *J Manuf Proc*. 2022;75:670–81.

**Publisher's Note** Springer Nature remains neutral with regard to jurisdictional claims in published maps and institutional affiliations.

Springer Nature or its licensor (e.g. a society or other partner) holds exclusive rights to this article under a publishing agreement with the author(s) or other rightsholder(s); author self-archiving of the accepted manuscript version of this article is solely governed by the terms of such publishing agreement and applicable law.